



Cite this: *Soft Matter*, 2016, 12, 1324

Received 11th September 2015,  
Accepted 10th November 2015

DOI: 10.1039/c5sm02299a

www.rsc.org/softmatter

## Experimental studies on the rheology of cubic blue phases†

Rasmita Sahoo,<sup>a</sup> O. Chojnowska,<sup>b</sup> R. Dabrowski<sup>b</sup> and Surajit Dhara<sup>\*a</sup>

We report detailed experimental studies on the rheology of cubic blue phases. We observe several flow regimes within each blue phase from rheomicroscopy and small angle light scattering experiments. Both the cubic blue phases exhibit solid-like response while the cholesteric phase shows gel-like behavior. The elastic modulus of BP-I is larger than that of BP-II. The shear induced yield transition occurs at a higher strain in BP-II than BP-I. Both the blue phases show stress relaxation through periodic modulation in step-strain experiments. Our results show that the rheological responses of these two phases are significantly different owing to the distinct networks of defect-disclinations.

### I. Introduction

In cholesteric liquid crystals the director (the average orientation direction of the molecules) spontaneously twists around a single helical axis of fixed orientation. In highly chiral systems, close to the isotropic transition, the orientation of the local director can twist around two perpendicular axes and the corresponding deformed structure is termed a “double-twist cylinder”.<sup>1</sup> Blue phases are special cases in which double twist cylinders fill up the volume by stabilizing a lattice of defect-disclinations.<sup>2,3</sup> Depending on the arrangement of the defect lines they are classified into three types namely, BP-I (body-centered cubic structure), BP-II (simple cubic) and BP-III (amorphous). The schematic diagrams of BP-I and BP-II which are the subject matter of investigation of this paper are shown in Fig. 1. The discovery of polymer stabilized blue phases with a wide temperature range has created a lot of interest owing to their possible applications.<sup>4–12</sup> Significant progress has also been made in various applications of blue phases. Nevertheless many fundamental aspects of these exotic phases are still unexplored. For example, recently several predictions were made on the rheological properties and the dynamics of the disclination networks of BP-I and BP-II.<sup>13–15</sup> However experimentally very little is known about the rheology of these phases.<sup>16–18</sup> In this paper, we report first detailed experimental studies on the rheology of cubic blue phases. Our results show that different rheological responses of BP-II and BP-I are connected to their structures and the dynamics of the defect networks.

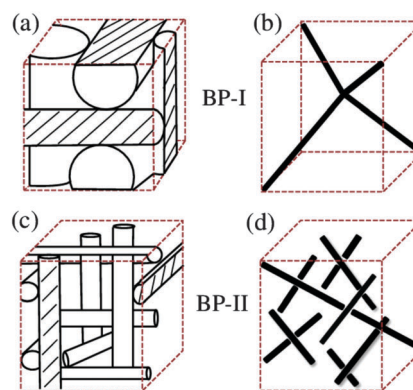


Fig. 1 Schematic diagrams of the BP-II and BP-I. (a and c) Spatial arrangements of double twisted cylinders in unit cells. (b) Simple cubic unit cell of the disclination lattice in BP-II. (d) Body centered cubic unit cell of the disclination lattice in BP-I. The black lines in (b) and (d) are the defect-disclinations.

### II. Experimental

The blue phase liquid crystal used in this study is a mixture of four fluorinated compounds and a highly chiral dopant. These compounds were synthesized in our laboratory. They are chemically stable and exhibit high resistivity.<sup>19</sup> The details of the molecular structure and their wt% are given in the supplementary.<sup>20</sup> It exhibits following phase transitions: I 46.4 °C BP-II 41.4 °C BP-I 36.6 °C N\*. Rheological measurements were performed using a controlled strain Rheometer (MCR 501, Anton Paar) with a cone-plate measuring system having a plate diameter of 25 mm and a cone angle of 1°. The temperature of the sample was controlled with an accuracy of 0.1 °C using a Peltier temperature controller. All the measurements were made upon cooling the sample from the isotropic phase.

<sup>a</sup> School of Physics, University of Hyderabad, Hyderabad-500046, India.  
E-mail: sdsp@uohyd.ernet.in

<sup>b</sup> Institute of Chemistry, Military University of Technology, 00-908 Warsaw, Poland

† Electronic supplementary information (ESI) available. See DOI: 10.1039/c5sm02299a

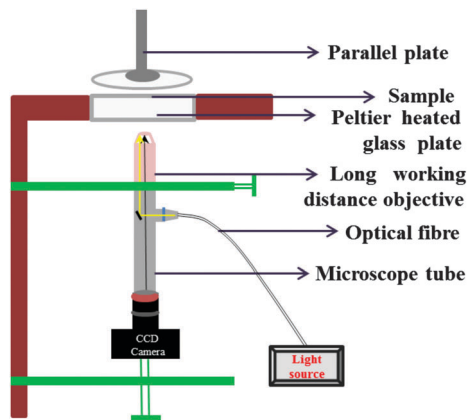


Fig. 2 Schematic diagram of the polarized light rheomicroscopy setup. The setup was attached under the bottom plate. The images are taken in the reflection mode.

We attached a microscope and a camera to the rheometer for optical rheo-microscopy. A schematic diagram of the setup is shown in Fig. 2. The rheomicroscopy setup consists of a CCD camera (monochrome), a microscope tube and a long working distance objective (NA = 0.4, 20 $\times$ , Nikon). We used parallel plate geometry of diameter 43 mm and the thickness of the bottom glass-plate is 6 mm. The sample was illuminated by using a polarized light through the objective from the bottom. An analyzer was placed in the microscope tube before the CCD camera. The microscope tube is adjustable in the  $y$  and  $z$  direction for focusing. The details of the small angle light scattering setup are given in ref. 21. The gap between two parallel glass plates in rheomicroscopy was 0.075 mm.

### III. Results and discussion

The bulk sample was mounted on the rheometer without any surface treatment of the measuring plates and the measurements were made while cooling the sample from the isotropic phase at 0.1  $^{\circ}\text{C min}^{-1}$ . To identify the phase transition temperatures in the rheometer we first measured the temperature dependent shear stress at a fixed shear rate (Fig. 3). The isotropic (I) to

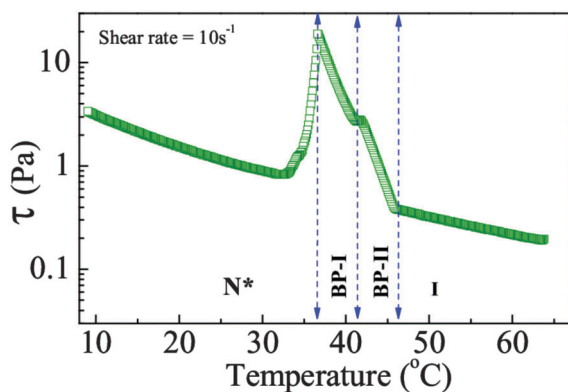


Fig. 3 Temperature dependent shear stress at a constant shear rate of 10  $\text{s}^{-1}$ . Three different phase transitions are marked by vertically dotted lines.

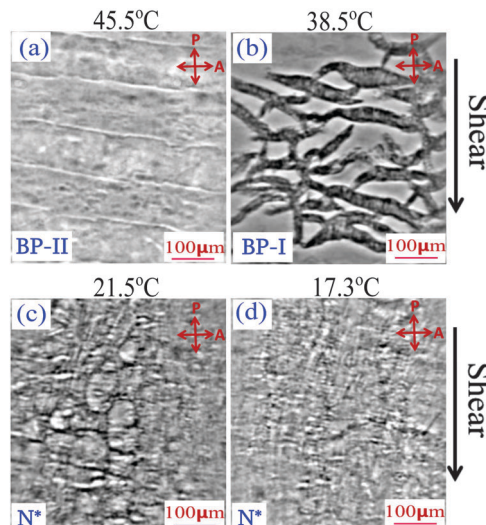


Fig. 4 Optical rheomicroscopy images taken during the measurement of temperature vs. shear stress at a constant shear rate of 10  $\text{s}^{-1}$  in three different phases. The direction of shear is shown by an arrow. P and A indicate crossed polarizers.

BP-II phase transition is marked by a rapid increase of the stress and the BP-I to cholesteric phase ( $N^*$ ) transition is marked by a sudden fall of the same. A small kink is observed at the BP-II to BP-I phase transition. The temperature range of BP-II and BP-I is 5  $^{\circ}\text{C}$  and 4.8  $^{\circ}\text{C}$ , respectively. The stress in the  $N^*$  is almost comparable to that of the isotropic phase except a gradual increase due to the decrease of temperature. It is observed that the shear stress of BP-I is larger than that of the BP-II and  $N^*$  phase.

Fig. 4 shows some representative rheomicroscopy images taken during the measurement of temperature dependent shear stress at a constant shear rate. In BP-II, the Grandjean-cano lines are observed which are oriented perpendicular to the shear direction (Fig. 4(a)). It suggests that the director is aligned parallel to the shear direction. The increase of stress compared to the isotropic phase is due to the motion of these Grandjean-cano lines. As the temperature is reduced, some filamentary structures appear in BP-I (Fig. 4(b)) and the stress also increased compared to BP-II. These filamentary structures are continuously broken and rejoined during the steady shear. The cholesteric phase shows a typical texture (Fig. 4(c) and (d)) similar to that usually observed under planar degenerate surface anchoring conditions.

The shear rate dependent viscosity and the corresponding rheomicroscopy images are shown in Fig. 5 and 6, respectively. We observe that the  $N^*$  phase exhibits a typical shear thinning behavior (Fig. 5(a)). The viscosity of BP-II and BP-I phases is much larger than that of the  $N^*$  phase in the low shear rate regime (0.01 to 1  $\text{s}^{-1}$ ). For example, at  $\dot{\gamma} = 0.01 \text{ s}^{-1}$ ,  $\eta_{N^*} = 1.2 \text{ Pa s}$ ,  $\eta_{BP-II} = 17 \text{ Pa s}$  and  $\eta_{BP-I} = 52 \text{ Pa s}$ . BP-I and BP-II show multiple shear thinning and finally the viscosity of BP-II at the highest shear rate is lower than that of the  $N^*$  phase. Thus BP-II shows stronger shear thinning behavior than the other two phases. The corresponding variation of shear stresses of three phases is

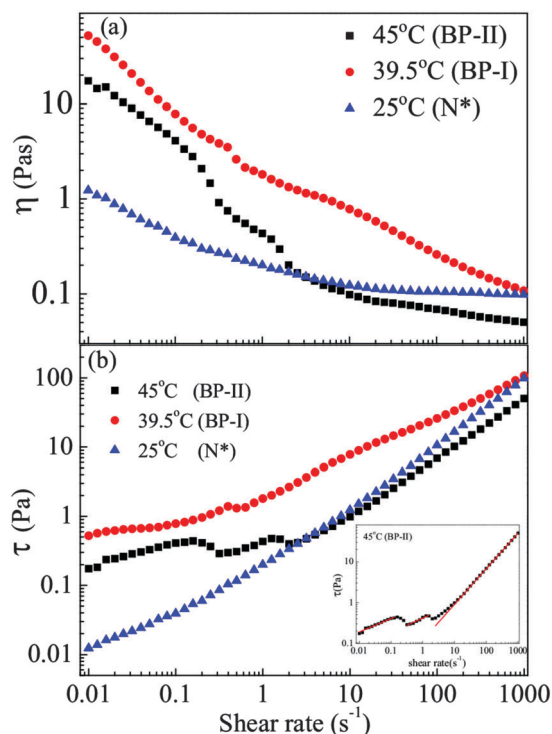


Fig. 5 Shear rate dependent (a) viscosity and (b) stress at three different temperatures. (inset) Red lines are best fits to the power law:  $\tau = a\dot{\gamma}^\alpha$ .

also shown in Fig. 5(b). Further we have also estimated the Ericksen number ( $E_r$ ) of the three phases. The range of Ericksen

numbers of the  $N^*$  phase is  $30 < E_r < 9 \times 10^4$  where the shear rate varies from 0.01 to  $1000 \text{ s}^{-1}$ . Similarly for the BP-II and BP-I, the ranges of Ericksen number are  $50 < E_r < 7 \times 10^4$  and  $300 < E_r < 1.2 \times 10^5$ , respectively.

Shear stress of BP-II shows three distinct regimes namely BP-II(1):  $\dot{\gamma} = 0.01\text{--}0.3 \text{ s}^{-1}$ ; BP-II(2):  $\dot{\gamma} = 0.3\text{--}2 \text{ s}^{-1}$  and BP-II(3):  $\dot{\gamma} = 2\text{--}1000 \text{ s}^{-1}$ . A power law fit  $\tau = a\dot{\gamma}^\alpha$  describes the data to a very good approximation. The fit parameters are:  $a = 0.87$  and  $\alpha = 0.33$  in BP-II(1);  $a = 0.42$  and  $\alpha = 0.35$  in BP-II(2);  $a = 0.12$  and  $\alpha = 0.87$  in BP-II(3). Some representative rheomicroscopy images in these regimes are also shown in Fig. 6. We observe that in BP-II(1), the Grandjean-cano lines flow parallel to the shear direction (downward green arrows in Fig. 6). In BP-II(2), the Grandjean-cano lines are broken and in BP-II(3) the texture appears like a flow aligned nematic phase. In BP-I, there are also several regimes but they are not distinctly separable as those of BP-II. Nevertheless it is clear that the multiple shear thinning is due to the breaking of texture at different shear rates (BP-I in Fig. 6). The cholesteric phase shows uniform shear thinning behavior and there is no significant change in the textures up to the shear rate of  $10 \text{ s}^{-1}$ . Beyond this shear rate the helix uncoils and leaves a flow induced nematic phase and hence the viscosity decreases. In the case of BP-II and BP-I, the flow induced nematic state appears at shear rates above 126 and  $200 \text{ s}^{-1}$ , respectively. Recently, Henrich *et al.* studied the rheology of cubic blue phases by numerical simulation.<sup>14</sup> Depending on the shear rate and the Ericksen number various flow regimes have been identified in both BP-I and BP-II. So our results qualitatively agree with their predictions.

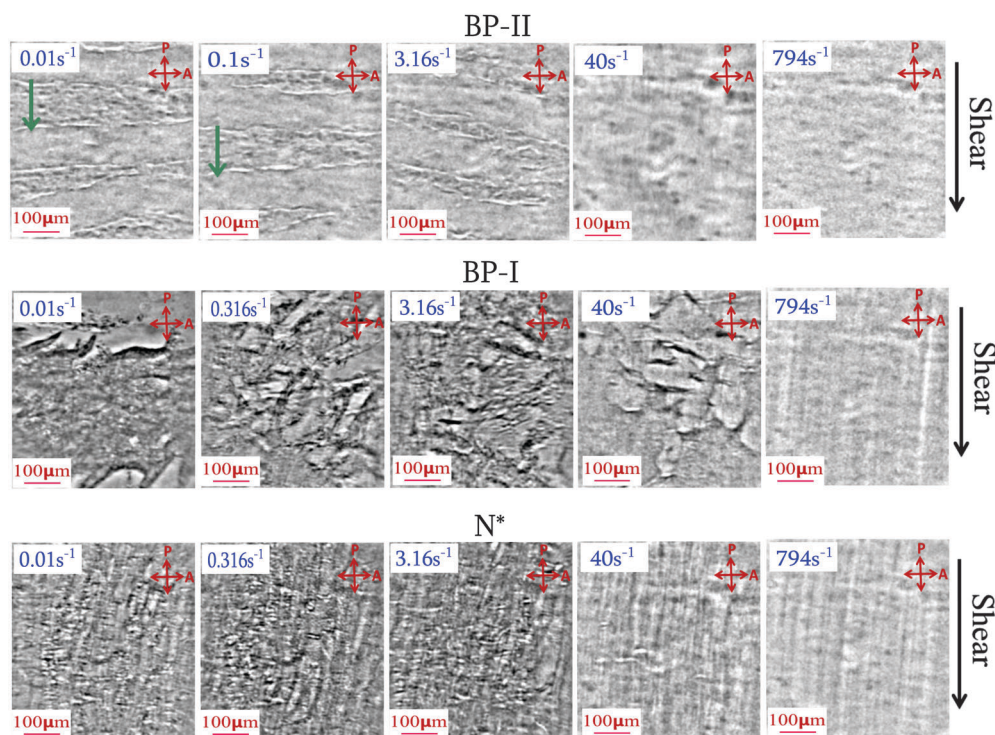


Fig. 6 Rheomicroscopy images taken during the measurement of shear rate dependent viscosity in three phases. The direction of shear is shown by an arrow on the right side. The downward green arrows in BP-II show the motion of the Grandjean-cano lines. See ESI† (Video S1).

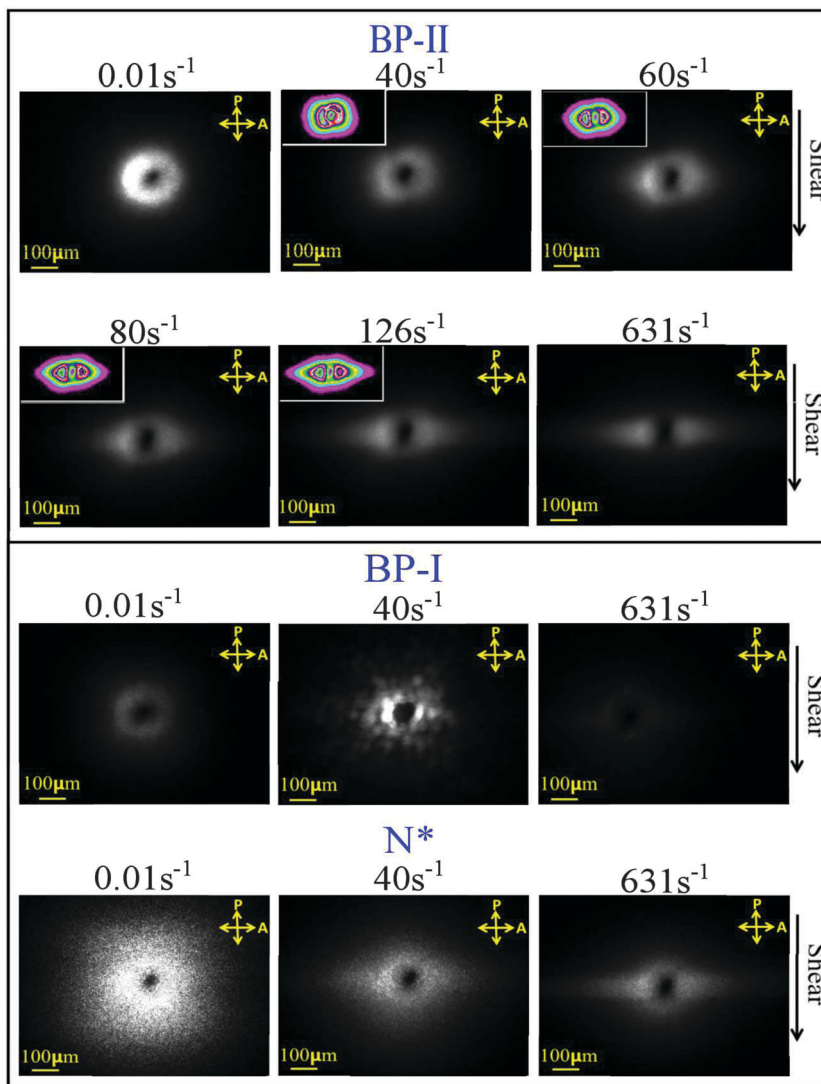


Fig. 7 Small angle light scattering (SALS) images taken in the  $H_V$  polarisation configuration at three different temperatures and various shear rates. The direction of shear is shown by an arrow. The insets are contour plots with false colours.

We also performed small angle light scattering (SALS) experiments. The details of the experimental setup were reported in ref. 21. The images of  $H_V$  scattering at various shear rates are shown in Fig. 7. We observe that the SALS patterns of all the phases at the lowest shear rate ( $0.01\text{ s}^{-1}$ ) are mostly circular with the largest diameter in the  $N^*$  phase. It suggests that the orientational fluctuations are stronger in the  $N^*$  phase compared to the other two phases. Interestingly at higher shear rates ( $40\text{--}126\text{ s}^{-1}$ ) BP-II shows obscure butterfly patterns. The butterfly patterns are prominently observed in contour plots (insets of Fig. 7). These kinds of SALS patterns are typically observed in complex fluids including polymer solutions, polymer mixtures, micellar surfactants and lyotropic lamellar phases due to the density or concentration fluctuations that are moderately coupled to the flow.<sup>22,23</sup> However we did not observe any special feature in rheomicroscopy at the same shear rates. It suggests that the characteristic time of flow is faster than the breaking and reforming of the microstructures.

At a shear rate of  $40\text{ s}^{-1}$ , BP-I shows multiple scattering patterns (Fig. 7, BP-I) which are very different from BP-II. This is due to the stronger orientational fluctuations caused by larger microstructures observed (Fig. 6, BP-I) in rheomicroscopy. At a shear rate of  $40\text{ s}^{-1}$ ,  $N^*$  shows an anisotropic scattering pattern that is elongated perpendicular to the shear direction. At a very high shear rate (e.g.,  $631\text{ s}^{-1}$ ), the scattering patterns of both BP-II and  $N^*$  phases are highly elongated perpendicular to the shear direction. Since the images are in the  $q$ -space, the overall alignment of the director is along the shear direction. The scattering intensity at a higher shear rate (for example, at  $631\text{ s}^{-1}$ ) in BP-I is almost zero and this could be due to the very low birefringence and ceasing of orientational fluctuations due to the large elastic modulus.

Fig. 8 shows the strain dependent storage ( $G'$ ) and the loss ( $G''$ ) moduli of all the phases. It is observed that in the  $N^*$  phase, in the low strain regime ( $\gamma \leq 1\%$ ),  $G' \simeq G''$ . In the high strain regime ( $\gamma > 1\%$ ),  $G''$  is larger than  $G'$  and it shows a

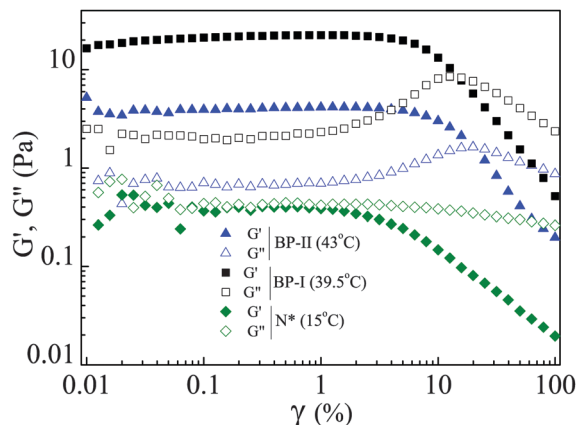


Fig. 8 The strain dependence of the storage  $G'$  and the loss  $G''$  moduli of the sample at three different temperatures where  $\omega = 1 \text{ rad s}^{-1}$ .

typical fluid-like behavior.  $G'$  of both the blue phases is higher than that of the  $N^*$  phase and  $G'$  of BP-I is around 5 times larger than that of BP-II. The linear viscoelastic (LVE) range of both the cubic phases is almost comparable (*i.e.*,  $\gamma_c = 4\%$ ). In BP-I, the strain induced fluidization or the yield transition ( $G' = G''$ ) occurs at  $\gamma = 16\%$  whereas in BP-II it occurs at a higher strain value ( $\gamma = 20\%$ ) than that of BP-I. This could be due to the fact that the defect lines in BP-II are intersecting and larger strain is needed to break the intersection and as a result its critical strain amplitude is higher than that of the BP-I.

To obtain more insight into the rheological response of the defect networks we performed step-strain measurements. Fig. 9 shows the stress response under applied step-strain. Here the strain value is changed from 0.3% (within LVE) to 30% (above LVE range). There are three regions in the time dependent shear stress. Initially (region-I) the strain is below the LVE range and constant for 600 s. Then the strain is increased above the LVE range (region-II) and constant for 600 s and again it is decreased to 0.3% (region-III). The  $N^*$  phase shows expected stress response under applied step-strain in all the regions. In

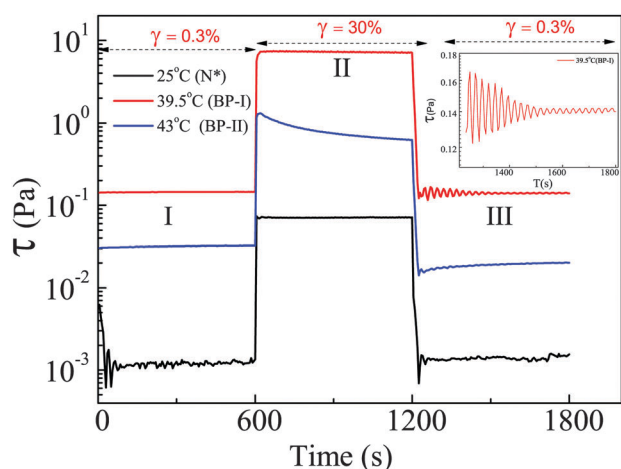


Fig. 9 Time dependent shear stress at three different temperatures. (inset) The periodic modulation in the BP-I, in region-III.

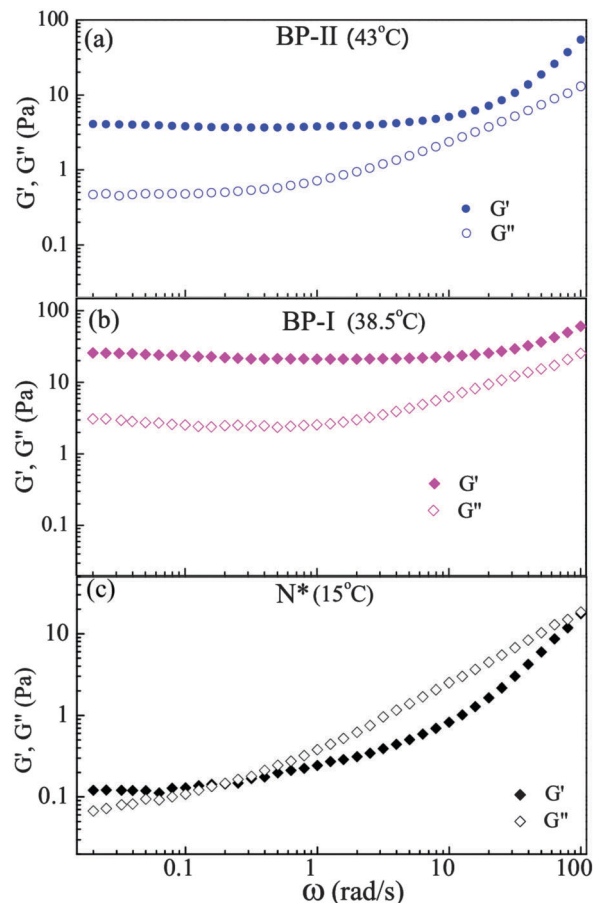


Fig. 10 The frequency dependence of the storage  $G'(\omega)$  and the loss  $G''(\omega)$  moduli of the sample at three different temperatures. The strain amplitude  $\gamma = 1\%$ .

region-II of BP-II there is a gradual decrease of stress with time and it could be due to the breaking of defect nodes under high strain followed by a continuous bulk flow. In the same region of BP-I the stress is constant where the system undergoes a flow aligned state. In this case there is no breaking of defect networks, as they do not intersect. In region-III both BP-I and BP-II show sinusoidal stress oscillations that decay with time. The amplitude of oscillation is more in BP-I than that of BP-II. Under a large strain the defects of BP-I are displaced from the equilibrium positions consequently the network is distorted and they tend to reorganize upon removal of the strain and this could lead to a periodic stress oscillation that decays with time. The small oscillation in region-III in BP-II could be due to the reconnection of some defects. We conjecture that the step-strain experiment clearly displays the different dynamical responses of BP-I and BP-II under large strain which are due to the different network structure of the defects.

Finally we have measured the frequency response of  $G'$  and  $G''$  of three phases (Fig. 10). The cholesteric phase exhibits a behavior very similar to that of a gel.<sup>24</sup> At low frequency ( $\omega < 0.2$ ),  $G'$  reaches a plateau where  $G_0 = 0.1 \text{ Pa}$ , and the elastic modulus is higher than the loss modulus. At higher frequency ( $\omega \geq 0.2$ ), a fluid like behavior is observed with

$G''$  being greater than  $G'$ . Thus there is a crossover at a critical frequency  $\omega = 0.2 \text{ rad s}^{-1}$ , from a solid-like regime where  $G' > G''$  and a fluid-like regime where  $G'' > G'$ . In the case of BP-II and BP-I,  $G'$  is always greater than  $G''$  and a plateau signifies a solid-like behavior of the two phases.

## IV. Conclusions

In conclusion, we have experimentally studied the rheological properties of cubic blue phases. Our experiment reveals several flow regimes with characteristic microstructures within each blue phase. At a high shear-rate regime all the phases exhibit a flow aligned nematic state. The measured apparent viscosity is larger in BP-I than in BP-II. In the step strain measurements BP-I exhibits decaying stress oscillation with time which is connected to the different dynamical response of the defect networks under large strain. The amplitude of the sinusoidal oscillations of BP-I in the step-strain experiment is larger than that of BP-II. These results are qualitatively in agreement with recent simulation. Both BP-II and BP-I exhibit a solid-like behavior while the cholesteric phase shows a gel-like behavior and the elastic modulus of BP-I is larger than that of BP-II. The larger critical strain for yield transition in BP-II is due to the breaking of defect nodes.

## Acknowledgements

We gratefully acknowledge the support of the CSIR (03(1207)/12/EMR-II). R. S. acknowledges UGC for the BSR fellowship. We acknowledge Dr Henrich for useful discussions and Dr J. Ananthaiah for help in setting SALS experiments. OC and RD acknowledge POIG (No. 01.03.01-14-016/08).

## References

- 1 P. G. de Gennes and J. Prost, *The Physics of Liquid crystals*, Oxford University Press, London, 2nd edn, 1993.
- 2 H. Grebel, R. M. Hornreich and S. Shtrikman, *Phys. Rev. A: At., Mol., Opt. Phys.*, 1984, **30**, 3264.
- 3 D. C. Wright and N. D. Mermin, *Rev. Mod. Phys.*, 1989, **61**, 385.
- 4 H. Kikuchi, M. Yokota, Y. Hisakado, H. Yang and T. Kajiyama, *Nat. Mater.*, 2002, **1**, 64.
- 5 H. J. Coles and M. N. Pivnenko, *Nature*, 2005, **436**, 997.
- 6 K. M. Chen, S. Gauza, H. Q. Xianyu and S. T. Wu, *J. Disp. Technol.*, 2010, **6**, 49.
- 7 D. P. Resler, D. S. Hobbs, R. C. Sharp, L. J. Friedman and T. A. Dorschner, *Opt. Lett.*, 1996, **21**, 689.
- 8 Y. H. Lin, H. S. Chen, H. C. Lin, Y. S. Tsou, H. K. Hsu and W. Y. Li, *Appl. Phys. Lett.*, 2010, **96**, 113505.
- 9 J. Yan, Y. Li and S. T. Wu, *Opt. Lett.*, 2011, **36**, 1404.
- 10 M. Mori, T. Hatada, K. Ishikawa, T. Saishouji, O. Wada, J. Nakamura and N. Terashima, *J. Soc. Inf. Display*, 1999, **7**, 257.
- 11 J. Yan and S. T. Wu, *Opt. Mater. Express*, 2011, **1**, 1527.
- 12 Y. Li, Y. Chen, J. Sun, S. T. Wu, S. H. Liu, P. J. Hsieh, K. L. Cheng and J. W. Shiu, *Appl. Phys. Lett.*, 2011, **99**, 181126.
- 13 O. Henrich, K. Stratford, D. Marenduzzo, P. V. Coveney and M. E. Cates, *J. Phys.: Condens. Matter*, 2012, **24**, 284127.
- 14 O. Henrich, K. Stratford, P. V. Coveney, M. E. Cates and D. Marenduzzo, *Soft Matter*, 2013, **9**, 10243.
- 15 A. Dupuis, D. Marenduzzo, E. Orlandini and J. M. Yeomans, *Phys. Rev. Lett.*, 2005, **95**, 097801.
- 16 R. N. Kleiman, D. J. Bishop, R. Pindak and P. Taborek, *Phys. Rev. Lett.*, 1984, **53**, 2137.
- 17 N. A. Clark, S. T. Vohra and M. A. Handschy, *Phys. Rev. Lett.*, 1984, **52**, 57.
- 18 M. Rajeswari, J. Ananthaiah, R. Dabrowski, V. S. S. Sastry, S. Dhara and B. K. Sadashiva, *Mol. Cryst. Liq. Cryst.*, 2011, **547**, 39.
- 19 O. Chojnowska, R. Dabrowski, J. Yan, Y. Chen and S. T. Wu, *J. Appl. Phys.*, 2014, **116**, 213505.
- 20 Supplementary materials at for the chemical structures of the compounds and the video (ESI†).
- 21 J. Ananthaiah, M. Rajeswari, V. S. S. Sastry, R. Dabrowski and S. Dhara, *Phys. Rev. E: Stat., Nonlinear, Soft Matter Phys.*, 2012, **86**, 011710.
- 22 E. K. Wheeler, P. Izu and G. G. Fuller, *Rheol. Acta*, 1996, **35**, 139.
- 23 B. Belzung, F. Lequeux, J. Vermant and J. Mewis, *J. Colloid Interface Sci.*, 2000, **224**, 179.
- 24 L. Ramos, M. Zapotocky, T. C. Lubensky and D. A. Weitz, *Phys. Rev. E: Stat., Nonlinear, Soft Matter Phys.*, 2002, **66**, 031711.